JACS
JOURNAL OF THE AMERICAN CHEMICAL SOCIETY
Communication
pubs.acs.org/JACS

Origins of Selectivity and General Model for Chiral Phosphoric Acid-Catalyzed Oxetane Desymmetrizations

Pier Alexandre Champagne and K. N. Houk*

Department of Chemistry and Biochemistry, University of California, Los Angeles, California 90095, United States

Supporting Information

ABSTRACT: The origins of the high enantioselectivity of chiral phosphoric acid-catalyzed oxetane desymmetrizations were investigated by density functional theory (DFT) calculations. Distortion of the catalyst structure, caused by steric crowding in the catalyst pocket of one enantiomeric transition state, is the main cause for stereochemical preference. A general model was developed to assist in the rational design of new catalysts for related transformations.

Chiral phosphoric acid (PA) catalysis is a powerful tool in asymmetric synthesis.[1] Catalysts of this class operate in most reactions through bifunctional activation, where the PA moiety serves both as a general acid and a general base (through the phosphoryl oxygen), simultaneously activating both the electrophile and nucleophile.[1,2] This versatile mode of action allows a wide range of applications for PA catalysis, mostly directed toward nucleophilic addition to sp^2 electrophiles (imines, carbonyls, etc.).[1] Multiple experimental and computational studies of such systems have produced models of selectivity that are based on the size and orientation of the catalyst's chiral pocket, favoring one enantiomeric transition state (TS).[3]

Application of PA catalysis to substitution reactions of sp^3 electrophiles is much less developed, although enantioselective openings of *meso*-aziridines[4] and epoxides,[5] azetidines[6] and oxetanes[7] are known. These reactions involve various nucleophiles, including thiols, carboxylic acids, alcohols, amines, and hydrogen chloride, and generate enantioenriched ring-opened alcohol or amine products that have great synthetic value. A model of selectivity for these reactions would help the rational design of new catalysts and their application to additional systems. Since TSs for nucleophilic substitutions at sp^3 centers have strikingly different geometries from TSs for additions to sp^2 electrophiles, previous models (such those developed by Goodman and others for imines)[2,3d,e] cannot be applied directly to sp^3 systems.

Recently, Seguin and Wheeler reported a theoretical study of PA-catalyzed openings of *meso*-epoxides and identified electrostatic interactions that control the modest selectivity.[8] We have now computationally investigated the origins of high enantioselectivity in oxetane openings and report a broadly applicable model based on our results.

We studied Sun and co-workers' most recent oxetane desymmetrization that uses HCl as the *in situ*-generated nucleophile (Scheme 1).[7e] SPINOL-derived catalysts **2** were found to be more selective than commonly used BINOL-derived PAs in this reaction. Using catalyst (*S*)-**2a**, the transformation is fast, highly selective, and has a wide substrate scope, making it an attractive entry-point to understand the whole class of oxetane opening reactions.

Scheme 1. Sun's Asymmetric Desymmetrization of 3-Substituted Oxetanes 1 with HCl as Nucleophile[7e]

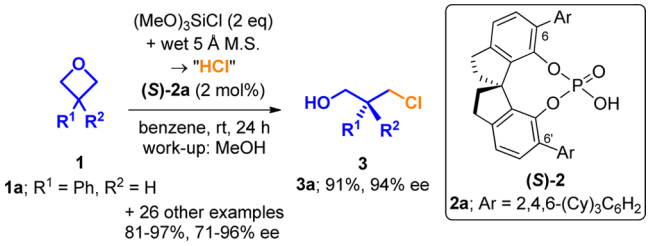

To elucidate the origins of stereoselectivity, we performed quantum chemical calculations[9] at the B3LYP-D3(BJ)/6-311+G(d,p)-CPCM(benzene)//B3LYP/6-31G(d) level of theory[10,11] using Gaussian 09.[12] These methods have been shown to give good results in related stereoselectivity studies.[3f−j,l,n,13,14] Structures were illustrated with CYLview.[15] Other DFT methods were also evaluated and are fully consistent with the trends and magnitudes of the relative activation free energies ($\Delta\Delta G^{\ddagger}$) presented in the main text.[9]

Assuming a bifunctional mode of activation, previously identified as operative in S_N2 reactions catalyzed by PAs,[8] we first investigated the reaction of oxetane **1a** with HCl, using phosphoric acid dimethyl ester **4** as a model catalyst. Three positions of the TS around the PA structure were located; the isoenergetic, lowest-energy **A** and **B** arrangements are shown as their Goodman projections[2] in Figure 1 (other projections are defined in Figure 3f). Both of these have the oxetane phenyl substituent *anti* to the PA catalyst. Arrangement **C** (not shown), with the oxetane substituent *syn* to the PA, is disfavored by 3.3 kcal/mol.[9] In all cases, the catalyst activates the nucleophilic Cl^- by deprotonating HCl and simultaneously activates the leaving group by protonation of the oxetane oxygen. Moreover, the expected linear nature of the S_N2 TS is slightly distorted, as the forming Cl−C bond makes a 159° angle with the breaking C−O bond.

We then explored the free energy profile of the reaction of **1a** catalyzed by (*S*)-**2a** (Figure 2). Binding of both substrates to the phosphoric acid of the catalyst generates a reactant-complex

Received: August 8, 2016
Published: September 14, 2016

DOI: 10.1021/jacs.6b08276
J. Am. Chem. Soc. 2016, 138, 12356−12359

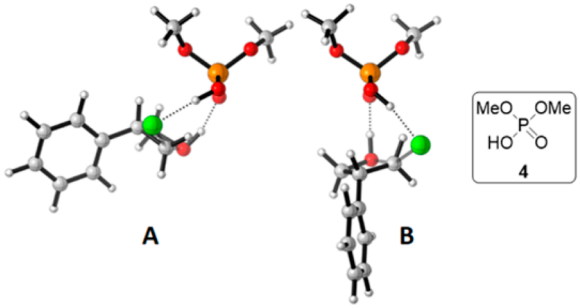

Figure 1. Lowest-energy TS arrangements for the reaction of oxetane **1a** with HCl, catalyzed by model PA **4**. The depicted TSs lead to the (*R*)-**3a** product.

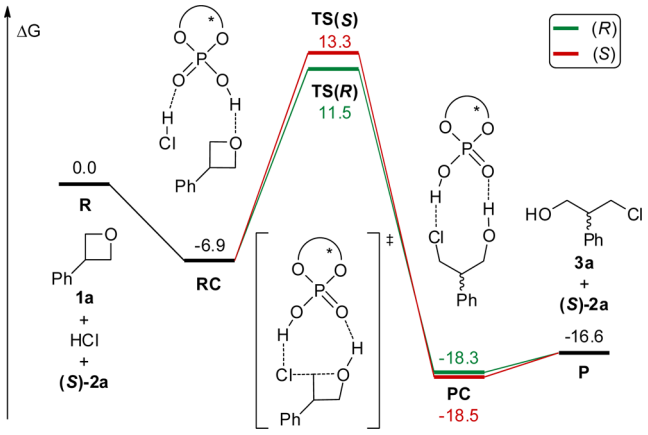

Figure 2. Free energy profile of the reaction of **1a** with HCl, catalyzed by (*S*)-**2a**. Energies are in kcal/mol.

(**RC**), which is 6.9 kcal/mol more stable than the separated reactants (**R**), due to strong hydrogen-bonding. From **RC**, the transformation is characterized by a single rate- and stereo-determining TS that combines C−O bond breaking, C−Cl bond formation, and proton shuttling from the nucleophile to the electrophile, assisted by the bifunctional nature of the PA. The lowest-energy TS leading to the preferred (*R*)-product (**TS**(*R*)) has a barrier of 18.4 kcal/mol and is 1.9 kcal/mol more stable than the corresponding TS leading to the (*S*)-product (**TS**(*S*)). Upon reaction, the product-complex (**PC**) is only 1.7 kcal/mol more stable than the free product **3a** (**P**), meaning quick turnover of the catalyst can be expected. These calculations are in excellent agreement with experimental observations, as they predict both the fast rates of the reaction at room temperature and the high level of enantioselectivity, measured at 94% ee ($\Delta\Delta G^{\ddagger}$ = 2.1 kcal/mol) for (*R*)-**3a**.[7e]

The lowest-energy conformations of **TS**(*R*) and **TS**(*S*) are shown below in their Goodman (Figure 3a,c) and Terada−Himo[3a,c] "quadrant" (Figure 3b,d) projections. The catalyst active site (PA moiety) is located in a chiral pocket, attached to the rigid 1,1′-spirobiindane backbone[16] and flanked by the 6,6′-aryl substituents (walls). Both **TS**(*R*) and **TS**(*S*) follow arrangement **B**, as any other organization of the TS, such as **A**, would incur strong steric clashes with the walls of the catalyst. In both cases, the acid of the PA protonates the oxetane oxygen, while the phosphoryl oxygen deprotonates HCl. Additionally, the Cl···C···O plane is tilted around 45° with respect with the O−P−O plane, in order to maximize these two acid−base interactions in the 8-membered proton-shuttling TS. Both TSs also have essentially identical bond distances and angles around this reaction site.

The most important difference between **TS**(*R*) and **TS**(*S*) is the absolute location and orientation of the catalyst walls (6,6′-aryls and their cyclohexyl substituents) and backbone

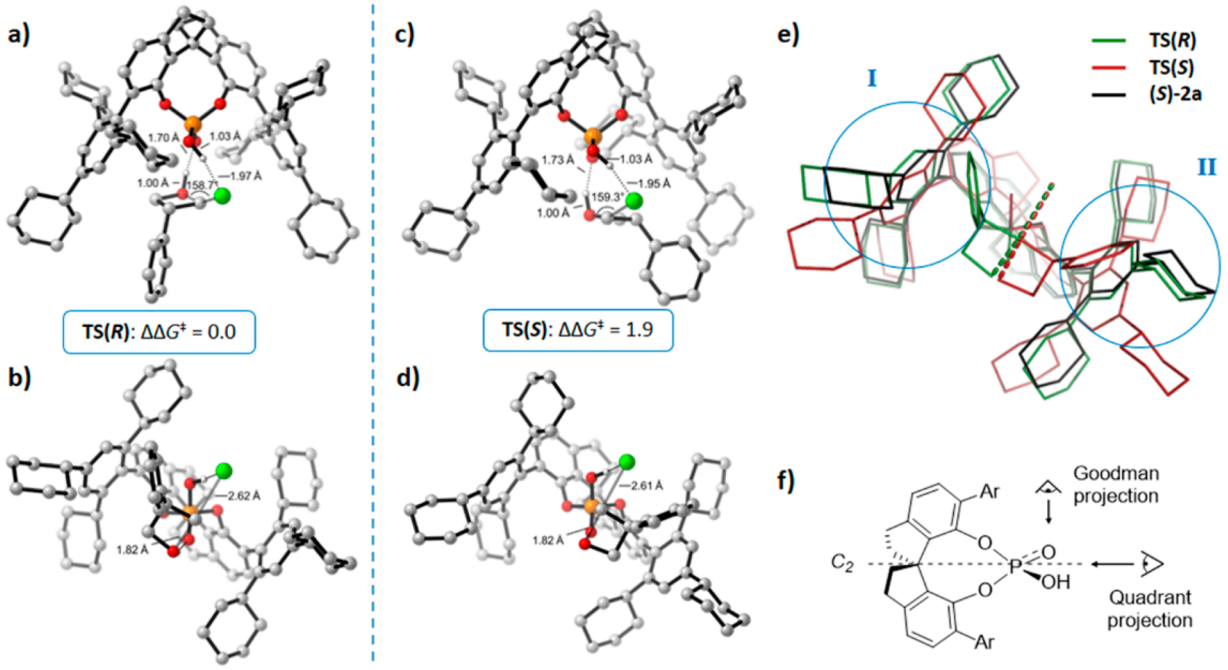

Figure 3. (a,c) Goodman projection of **TS**(*R*) and **TS**(*S*), respectively. (b,d) Quadrant projection of these TSs. Key bond lengths and angles are shown. Energies are in kcal/mol. (e) Superimposition of the quadrant projections of catalyst (*S*)-**2a** (black lines), **TS**(*R*) (green lines), and **TS**(*S*) (red lines). Blue circles, labeled **I** and **II**, highlight important steric interactions. (f) Definition of the Goodman and quadrant projections. In all panels, noncritical hydrogen atoms are omitted for clarity.

DOI: 10.1021/jacs.6b08276
J. Am. Chem. Soc. 2016, 138, 12356−12359

(spirobiindane), relative to the substrates. This effect is most easily seen using the quadrant projections (Figure 3b,d), in which the cyclohexyls in **TS(*S*)** have a significantly shifted position compared to **TS(*R*)**. To better demonstrate this twisting of the catalyst structure, the quadrant projections of **TS(*R*)**, **TS(*S*)**, and the free catalyst (*S*)-**2a** are overlaid in Figure 3e. Introduction of the substrates in the catalyst pocket, when organized as to form the (*R*)-product, incurs minimal reorganization of the catalyst structure, as hardly any steric crowding develops (highlight **I**). This is indicated by the almost perfectly superimposed structures of **TS(*R*)** (green) and the unperturbed conformation of the free catalyst (*S*)-**2a** (black). However, introduction of the substrates as in **TS(*S*)** (red) would cause major steric repulsions between the oxetane phenyl substituent and the cyclohexyl chain present at the *para* position of the free catalyst wall (black), as shown in highlight **II** of Figure 3e. Instead, the catalyst walls in **TS(*S*)** move away from the substrates, leading to the visible difference between the red and black structures in Figure 3e.

The nature and energetic cost of this catalyst distortion were investigated using a distortion/interaction analysis.[9,17] Single-point calculations in the gas-phase at the B3LYP-D3(BJ)/6-311+G(d,p) level were used to evaluate the relative roles of catalyst and substrates distortion and interaction on the overall energy difference ($\Delta\Delta E^{\ddagger} = \Delta E^{\ddagger}_{TS(S)} - \Delta E^{\ddagger}_{TS(R)}$) between **TS(*R*)** and **TS(*S*)**, which is 2.0 kcal/mol using this method. The calculated distortion energy difference is 2.1 kcal/mol for the catalyst fragment and −0.5 kcal/mol for the substrate fragment. The interaction energy difference is only 0.5 kcal/mol, indicating no significant difference in electrostatic interactions. By contrast, the Wheeler group found electrostatic interactions to be controlling in epoxide opening reactions.[8] From the above analysis, we recognize that the energy difference between the (*R*) and (*S*) pathways is mostly due to the greater distortion energy of the catalyst in the **TS(*S*)** structure.

Although it arises from steric repulsions between the substrate and catalyst walls, the greater distortion energy in **TS(*S*)** cannot be attributed to unfavorable conformations of the walls. To prove this, we truncated both **TS(*R*)** and **TS(*S*)** by replacing the 6,6′-aryl substituents (walls) of the catalyst with hydrogens, then calculated the resulting single-point $\Delta\Delta E^{\ddagger}$ without optimization.[9] The difference is still 2.0 kcal/mol. Therefore, although van der Waals repulsions force the cyclohexyls away from the substrate in **TS(*S*)**, this shifting actually induces twisting and strain into the spirobiindane backbone and phosphate group, forcing them to adopt conformations distorted from their most stable arrangements. The lower enantioselectivity exhibited in this reaction by BINOL-derived catalysts can thus be explained by their more flexible 1,1′-biaryl-based backbones, which allow them to better adjust to the strain induced by substrate binding.

We propose the following general model to explain and predict the stereochemical outcome in reactions of oxetanes catalyzed by axially chiral phosphoric acids (Figure 4). This model is based on the quadrant projection, which allows clear visualization of an S_N2 TS. The model depicted in Figure 4 accounts for (*R*)-BINOL- (and derivatives) or (*S*)-SPINOL-derived catalysts, which have the same sense of axial chirality.

We have shown that arrangement **B** (Figure 1) is preferred for both enantiomeric TSs (see Figure 3a,c). This aligns the substrate reaction plane in a way to position both the nucleophile and leaving group in the empty quadrants.[18] This is the key feature from which the whole model is built. Arrangement **B** also orients the largest substituent on the oxetane *anti* to the catalyst structure. From there, two enantiomeric TSs can be sketched.

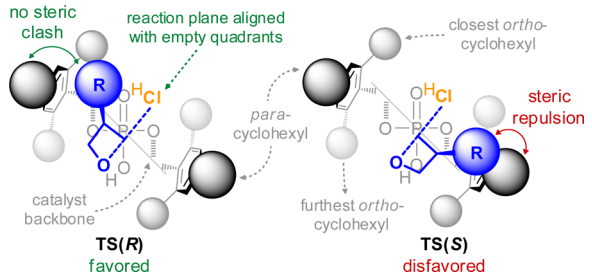

Figure 4. Model for oxetane desymmetrizations catalyzed by (*R*)-BINOL- or (*S*)-SPINOL-derived phosphoric acids. Steric repulsion analysis predicts that **TS(*R*)** will be favored.

The TS that would suffer from maximal steric repulsions between the substituent of the oxetane (blue sphere) and the substituents at the *para* position of the catalyst walls (black spheres) is predicted to be disfavored. Indeed, removal of these strong van der Waals interactions will occur by distortion of the catalyst structure, inducing unfavorable conformations in its backbone.

Our model can be further simplified to a "back-of-the-envelope" variant and can be applied to explain the stereochemical outcome of other asymmetric oxetane openings, without requiring additional computations (Figure 5). For

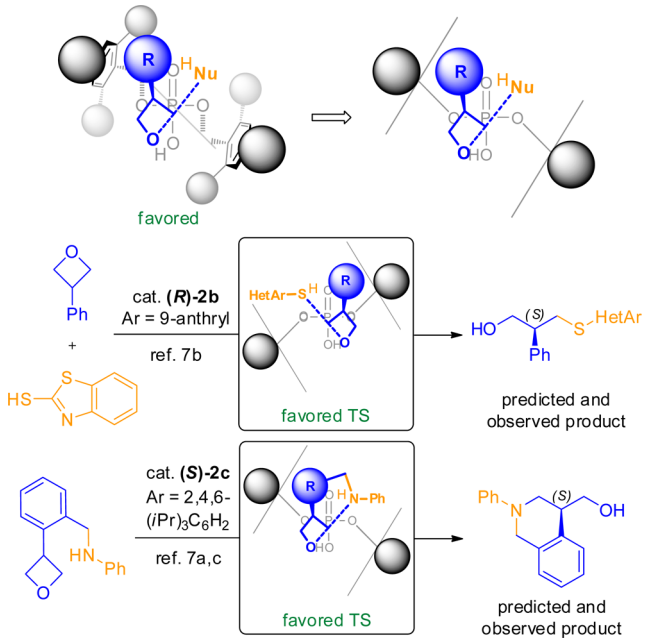

Figure 5. "Back-of-the-envelope" model applied to other enantioselective oxetane desymmetrizations. See Figure 1 for structure of catalyst **2**.

example, the major enantiomer resulting from both an intermolecular reaction with 2-mercaptobenzothiazole[7b] and an intramolecular amination[7a,c] are accurately explained by our simple steric analysis. Generalization of this model to reactions of disubstituted oxetanes and other sp^3 electrophiles is underway.

In summary, the enantioselective desymmetrization of oxetanes is controlled by steric interactions that ultimately cause unfavorable catalyst distortion. This also explains why SPINOL-derived PAs are more selective than their BINOL-derived variants for the reaction studied here, as BINOLs have more flexible structures. As S_N2 TSs are linear and align in predictable fashion in the pockets of chiral PAs, a simple model

DOI: 10.1021/jacs.6b08276
J. Am. Chem. Soc. 2016, 138, 12356−12359

to explain and predict selectivity was developed. We anticipate that it will spur new rationally designed catalysts and transformations in the important field of chiral PA catalysis.

■ ASSOCIATED CONTENT

Supporting Information

The Supporting Information is available free of charge on the ACS Publications website at DOI: 10.1021/jacs.6b08276.

Complete list of authors in the Gaussian 09 reference, full computational details and additional figures. Cartesian coordinates, energies, free energies, and number of imaginary frequencies of all stationary points and values of imaginary frequencies of all transition structures (PDF)

■ AUTHOR INFORMATION

Corresponding Author

*houk@chem.ucla.edu

Notes

The authors declare no competing financial interest.

■ ACKNOWLEDGMENTS

P.A.C. gratefully acknowledges the Fonds de recherche du Québec, Nature et Technologies (FRQNT) for a postdoctoral fellowship. We are grateful to the NSF (CHE-1361104 to K.N.H.) for financial support of this research. Computations were performed on the Hoffman2 cluster at UCLA and the Extreme Science and Engineering Discovery Environment (XSEDE), which is supported by the NSF (OCI-1053575). We thank Peiyuan Yu, Dr. Yu-hong Lam, and Dr. Matthew Grayson for helpful discussions regarding this work.

■ REFERENCES

(1) For reviews, see (a) Akiyama, T. *Chem. Rev.* **2007**, *107*, 5744. (b) Terada, M. *Synthesis* **2010**, *2010*, 1929. (c) Parmar, D.; Sugiono, E.; Raja, S.; Rueping, M. *Chem. Rev.* **2014**, *114*, 9047.

(2) Reid, J. P.; Simón, L.; Goodman, J. M. *Acc. Chem. Res.* **2016**, *49*, 1029.

(3) For selected examples, see (a) Gridnev, I. D.; Kouchi, M.; Sorimachi, K.; Terada, M. *Tetrahedron Lett.* **2007**, *48*, 497. (b) Yamanaka, M.; Itoh, J.; Fuchibe, K.; Akiyama, T. *J. Am. Chem. Soc.* **2007**, *129*, 6756. (c) Marcelli, T.; Hammar, P.; Himo, F. *Chem. - Eur. J.* **2008**, *14*, 8562. (d) Simón, L.; Goodman, J. M. *J. Org. Chem.* **2010**, *75*, 589. (e) Simón, L.; Goodman, J. M. *J. Org. Chem.* **2011**, *76*, 1775. (f) Hirata, T.; Yamanaka, M. *Chem. - Asian J.* **2011**, *6*, 510. (g) Grayson, M. N.; Pellegrinet, S. C.; Goodman, J. M. *J. Am. Chem. Soc.* **2012**, *134*, 2716. (h) Grayson, M. N.; Goodman, J. M. *J. Am. Chem. Soc.* **2013**, *135*, 6142. (i) Shibata, Y.; Yamanaka, M. *J. Org. Chem.* **2013**, *78*, 3731. (j) Wang, H.; Jain, P.; Antilla, J. C.; Houk, K. N. *J. Org. Chem.* **2013**, *78*, 1208. (k) Ajitha, M. J.; Huang, K.-W. *Org. Biomol. Chem.* **2015**, *13*, 10981. (l) Liu, C.; Besora, M.; Maseras, F. *Chem. - Asian J.* **2016**, *11*, 411. (m) Simón, L.; Paton, R. S. *Org. Biomol. Chem.* **2016**, *14*, 3031. (n) Reid, J. P.; Goodman, J. M. *J. Am. Chem. Soc.* **2016**, *138*, 7910.

(4) (a) Rowland, E. B.; Rowland, G. B.; Rivera-Otero, E.; Antilla, J. C. *J. Am. Chem. Soc.* **2007**, *129*, 12084. (b) Sala, G. D.; Lattanzi, A. *Org. Lett.* **2009**, *11*, 3330. (c) Larson, S. E.; Baso, J. C.; Li, G.; Antilla, J. C. *Org. Lett.* **2009**, *11*, 5186. (d) Senatore, M.; Lattanzi, A.; Santoro, S.; Santi, C.; Sala, G. D. *Org. Biomol. Chem.* **2011**, *9*, 6205. (e) Monaco, M. R.; Poladura, B.; Diaz de Los Bernardos, M.; Leutzsch, M.; Goddard, R.; List, B. *Angew. Chem., Int. Ed.* **2014**, *53*, 7063.

(5) (a) Wang, Z.; Law, W. K.; Sun, J. *Org. Lett.* **2013**, *15*, 5964. (b) Monaco, M. R.; Prévost, S.; List, B. *Angew. Chem., Int. Ed.* **2014**, *53*, 8142. (c) Monaco, M. R.; Prévost, S.; List, B. *J. Am. Chem. Soc.* **2014**, *136*, 16982.

(6) Wang, Z.; Sheong, F. K.; Sung, H. H. Y.; Williams, I. D.; Lin, Z.; Sun, J. *J. Am. Chem. Soc.* **2015**, *137*, 5895.

(7) (a) Chen, Z.; Wang, B.; Wang, Z.; Zhu, G.; Sun, J. *Angew. Chem., Int. Ed.* **2013**, *52*, 2027. (b) Wang, Z.; Chen, Z.; Sun, J. *Angew. Chem., Int. Ed.* **2013**, *52*, 6685. (c) Chen, Z.; Wang, Z.; Sun, J. *Chem. - Eur. J.* **2013**, *19*, 8426. (d) Yang, W.; Sun, J. *Angew. Chem., Int. Ed.* **2016**, *55*, 1868. (e) Yang, W.; Wang, Z.; Sun, J. *Angew. Chem., Int. Ed.* **2016**, *55*, 6954.

(8) Seguin, T. J.; Wheeler, S. E. *ACS Catal.* **2016**, *6*, 2681.

(9) See the Supporting Information for full computational details.

(10) (a) Becke, A. D. *J. Chem. Phys.* **1993**, *98*, 5648. (b) Lee, C.; Yang, W.; Parr, R. G. *Phys. Rev. B: Condens. Matter Mater. Phys.* **1988**, *37*, 785. (c) Vosko, S. H.; Wilk, L.; Nusair, M. *Can. J. Phys.* **1980**, *58*, 1200. (d) Stephens, P. J.; Devlin, F. J.; Chabalowski, C. F.; Frisch, M. J. *J. Phys. Chem.* **1994**, *98*, 11623.

(11) (a) Grimme, S.; Antony, J.; Ehrlich, S.; Krieg, H. *J. Chem. Phys.* **2010**, *132*, 154104. (b) Grimme, S.; Ehrlich, S.; Goerigk, L. *J. Comput. Chem.* **2011**, *32*, 1456. (c) Johnson, E. R.; Becke, A. D. *J. Chem. Phys.* **2006**, *124*, 174104. (d) Johnson, E. R.; Becke, A. D. *J. Chem. Phys.* **2005**, *123*, 024101. (e) Cossi, M.; Rega, N.; Scalmani, G.; Barone, V. *J. Comput. Chem.* **2003**, *24*, 669.

(12) Frisch, M. J.; et al. *Gaussian 09*, revision D.01; Gaussian, Inc.: Wallingford, CT, 2013.

(13) (a) Simón, L.; Goodman, J. M. *Org. Biomol. Chem.* **2011**, *9*, 689. (b) Lam, Y.-h.; Grayson, M. N.; Holland, M. C.; Simon, A.; Houk, K. N. *Acc. Chem. Res.* **2016**, *49*, 750.

(14) For additional recent examples, see: (a) Grayson, M. N.; Goodman, J. M. *J. Org. Chem.* **2013**, *78*, 8796. (b) Lam, Y.-h.; Houk, K. N. *J. Am. Chem. Soc.* **2014**, *136*, 9556. (c) Grayson, M. N.; Goodman, J. M. *J. Org. Chem.* **2015**, *80*, 2056. (d) Krenske, E. H.; Houk, K. N.; Harmata, M. *J. Org. Chem.* **2015**, *80*, 744. (e) Lam, Y.-h.; Houk, K. N. *J. Am. Chem. Soc.* **2015**, *137*, 2116. (f) Rodríguez, E.; Grayson, M. N.; Asensio, A.; Barrio, P.; Houk, K. N.; Fustero, S. *ACS Catal.* **2016**, *6*, 2506. (g) Simon, A.; Lam, Y.-h.; Houk, K. N. *J. Am. Chem. Soc.* **2016**, *138*, 503.

(15) Legault, C. Y. *CYLview*, 1.0b; Université de Sherbrooke, 2009 (http://www.cylview.org).

(16) Birman, V. B.; Rheingold, A. L.; Lam, K.-C. *Tetrahedron: Asymmetry* **1999**, *10*, 125.

(17) (a) Ess, D. H.; Houk, K. N. *J. Am. Chem. Soc.* **2007**, *129*, 10646. (b) Ess, D. H.; Houk, K. N. *J. Am. Chem. Soc.* **2008**, *130*, 10187.

(18) Since catalysts of this class are C_2-symmetric, the absolute position of the nucleophile and leaving group can be freely interchanged.

DOI: 10.1021/jacs.6b08276
J. Am. Chem. Soc. 2016, 138, 12356−12359